Inorganic Chemistry

Article

pubs.acs.org/IC

Influence of Ligand Flexibility on the Electronic Structure of Oxidized Ni^{III}-Phenoxide Complexes

Minoru Kawai,[†,‡] Takahide Yamaguchi,[‡] Shigeyuki Masaoka,[§] Fumito Tani,[∥] Takamitsu Kohzuma,[‡] Linus Chiang,[⊥] Tim Storr,[⊥] Kaoru Mieda,[#] Takashi Ogura,[#] Robert K. Szilagyi,[&,∇] and Yuichi Shimazaki*[,†]

[†]College of Science and [‡]Graduate School of Science and Engineering, Ibaraki University, Bunkyo, Mito 310-8512, Japan

[§]Institute for Molecular Science, Myodaiji, Okazaki 444-8585, Japan

[∥]Institute for Materials Chemistry and Engineering, Kyushu University, Higashi-ku, Fukuoka 812-8581, Japan

[⊥]Department of Chemistry, Simon Fraser University, Burnaby, British Columbia V5A 1S6, Canada

[#]Picobiology Institute, Graduate School of Life Science, University of Hyogo, Sayo, Hyogo 679-5184, Japan

[&]Department of Chemistry, Montana State University, Bozeman, Montana 59717, United States

Supporting Information

ABSTRACT: One-electron-oxidized Ni^{III}-phenoxide complexes with salen-type ligands, $[Ni(salen)py_2]^{2+}$ ($[\mathbf{1}^{en}\text{-}\mathbf{py}]^{2+}$) and $[Ni(1,2\text{-}salcn)py_2]^{2+}$ ($[\mathbf{1}^{cn}\text{-}\mathbf{py}]^{2+}$), with a five-membered chelate dinitrogen backbone and $[Ni(salpn)py_2]^{2+}$ ($[\mathbf{2}^{pn}\text{-}\mathbf{py}]^{2+}$), with a six-membered chelate backbone, have been characterized with a combination of experimental and theoretical methods. The five-membered chelate complexes $[\mathbf{1}^{en}\text{-}\mathbf{py}]^{2+}$ and $[\mathbf{1}^{cn}\text{-}\mathbf{py}]^{2+}$ were assigned as Ni^{III}-phenoxyl radical species, while the six-membered chelate complex $[\mathbf{2}^{pn}\text{-}\mathbf{py}]^{2+}$ was concluded to be a Ni^{II}-bis(phenoxyl radical) species with metal-centered reduction in the course of the one-electron oxidation of the Ni^{III}-phenoxide complex $[\mathbf{2}^{pn}\text{-}\mathbf{py}]^{+}$. Thus, the oxidation state of the one-electron-oxidized Ni^{III} salen-type complexes depends on the chelate ring size of the dinitrogen backbone.

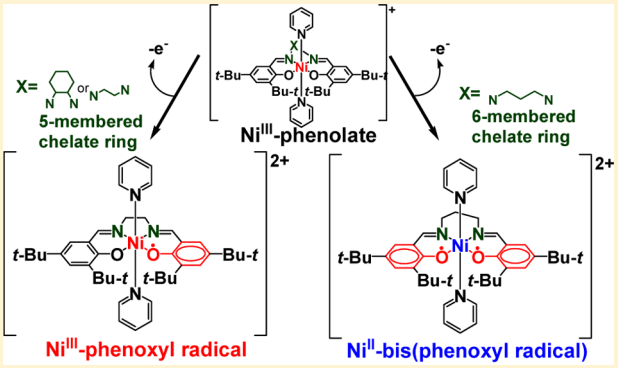

1. INTRODUCTION

The oxidation chemistry of metal complexes with redox-active ligands has been widely developed in recent years, affording insights into reaction mechanisms.[1] In particular, the tyrosyl radical has attracted much attention, due to its role as an organic redox-active cofactor in galactose oxidase (GO).[2,3] GO is a mononuclear copper oxidase that catalyzes the two-electron oxidation of primary alcohols to aldehydes, and the active form of GO exists as a Cu^{II}-phenoxyl radical.[4,5] In general, an "experimental" valence state of a metal complex could be different from the "formal" oxidation state, especially in species containing redox-active ligands.[1,3,4,6,7] Depending on the relative energies of the redox-active orbitals, metal complexes with noninnocent ligands can be assigned to two limiting descriptions, either metal−ligand radical ($M^{n+}(L^{\bullet})$) or high-valent metal−anionic ligand ($M^{(n+1)+}(L^{-})$) complexes.[7−12]

One-electron-oxidized nickel(II) salen-type complexes are known to exist in either form, depending on the salen ligand composition and availability of additional coordinating ligands.[13−18] The coordination geometry of the nickel ion determines that the oxidation locus on square-planar four-coordinate Ni^{II}-phenoxide complexes is dominantly the phenolate moiety, affording a Ni^{II}-phenoxyl radical species, whereas addition of exogenous ligands affords five- or six-coordinate complexes leading to a Ni^{III}-phenoxide species.[13−21]

Many other redox-active group 10 complexes, especially those containing Pd or Pt complexes, have been reported as catalysts for conversion of organic substrates[22] and as antitumor-active complexes.[23,24] In these complexes, the metal valence states can reach +IV.[25] Although some Ni complexes of +IV formal oxidation state have been previously reported as intermediates in catalytic reactions,[26] few high-valent Ni(IV) species have been characterized. Further, Ni enzymes exhibit oxidation states from Ni^{I} to Ni^{III} during catalysis, with no evidence for the +IV oxidation state.[24,27] Therefore, characterization of the electronic structure of high-valent Ni complexes could lead to the development of new catalytic reactivity.

Interestingly, two-electron-oxidized Ni^{II} complexes show different valence states, reflecting the "formal" and "experimental" oxidation states.[28,29] For example, some two-electron-

Received: May 20, 2014
Published: September 25, 2014

   dx.doi.org/10.1021/ic501181k | Inorg. Chem. 2014, 53, 10195−10202

oxidized Ni^{II} complexes containing phenoxide ligands can be assigned to a Ni^{II}-bis(phenoxyl radical) species.[6,29] Recently, a one-electron-oxidized Ni^{III} complex containing a Schiff base ligand with two phenoxide moieties was reported, but the "experimental" valence state of the oxidized complex could not be determined.[20] Obtaining nickel complexes of higher valence states is still a challenge in coordination chemistry.

Herein we present the valence state of a series of one-electron oxidized nickel(III) phenoxide complexes with five- and six-membered dinitrogen chelate backbones: $[Ni(salen)py_2]^{2+}$ ($[\mathbf{1}^{en}\text{-}\mathbf{py}]^{2+}$; Scheme 1), $[Ni(1,2\text{-}salcn)py_2]^{2+}$ ($[\mathbf{1}^{cn}\text{-}\mathbf{py}]^{2+}$), and $[Ni(salpn)py_2]^{2+}$ ($[\mathbf{2}^{pn}\text{-}\mathbf{py}]^{2+}$). The six-membered chelate Ni^{III}-phenoxide complex $[\mathbf{2}^{pn}\text{-}\mathbf{py}]^{+}$ is more distorted than both $[\mathbf{1}^{en}\text{-}\mathbf{py}]^{+}$ and $[\mathbf{1}^{cn}\text{-}\mathbf{py}]^{+}$, while their physicochemical properties are similar.[15,17] One-electron oxidation of these Ni^{III}-phenoxide precursors has been concluded to afford complexes with different electronic structures depending on the dinitrogen chelate ring size; $[\mathbf{1}^{en}\text{-}\mathbf{py}]^{2+}$ and $[\mathbf{1}^{cn}\text{-}\mathbf{py}]^{2+}$ are the first examples of Ni^{III}-phenoxyl radical complexes, while $[\mathbf{2}^{pn}\text{-}\mathbf{py}]^{2+}$ is a Ni^{II}-bis(phenoxyl radical) species formed with concomitant reduction of the Ni^{III} center.

Scheme 1. Structures of the salen-Type Five-Membered Dinitrogen Chelate Complexes Ni(salen) ($\mathbf{1}^{en}$) and Ni(1,2-salcn) ($\mathbf{1}^{cn}$) and Six-Membered Dinitrogen Chelate Complexes Ni(salpn) ($\mathbf{2}^{pn}$) and One-Electron Oxidation of Their Ni^{III} Complexes

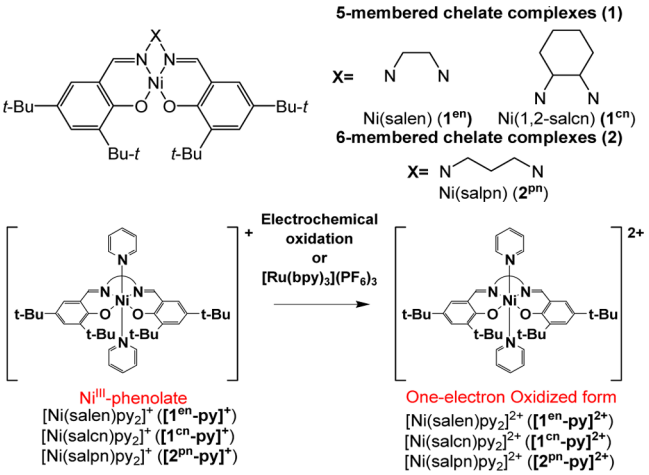

2. EXPERIMENTAL SECTION

2.1. Syntheses of Ni Complexes. Synthesis of the Ni^{II} complexes Ni(1,2-salcn) ($\mathbf{1}^{cn}$) and Ni(salpn) ($\mathbf{2}^{pn}$) and their one-electron-oxidized complexes $[Ni(salen)]SbF_6$ ($[\mathbf{1}^{en}]^+$), $[Ni(salcn)]SbF_6$ ($[\mathbf{1}^{cn}]^+$), and $[Ni(salpn)]SbF_6$ ($[\mathbf{2}^{pn}]^+$) have been reported previously.[16,17] The Ni^{III} complexes $[Ni(salen)py_2]SbF_6$ ($[\mathbf{1}^{en}\text{-}\mathbf{py}]^+$), $[Ni(1,2\text{-}salcn)py_2]SbF_6$ ($[\mathbf{1}^{cn}\text{-}\mathbf{py}]^+$), and $[Ni(salpn)]SbF_6$ ($[\mathbf{2}^{pn}\text{-}\mathbf{py}]^+$) were prepared by addition of 50 equiv of pyridine to CH_2Cl_2 solutions of $[\mathbf{1}]^+$ and $[\mathbf{2}]^+$.[16,17]

2.2. General Methods. UV−vis−NIR spectra were obtained with a JASCO V-670 spectrophotometer, equipped with a liquid nitrogen cooled cryostat (UNISOKU CoolSpeK UV USP-203-A), from −80 to +30 °C. EPR spectra were collected by using a Bruker EMXplus spectrometer operating with a premium X-band (9.5 GHz) microwave bridge. Low-temperature measurements of frozen solutions were carried out by using a Bruker helium temperature-control system and a continuous-flow cryostat. Samples for X-band measurements were placed in outer-diameter sample tubes (4 mm) with sample volumes of 300 μL. Electrolysis and cyclic voltammetry (CV) was performed on a HOKUTO DENKO HZ-5000 automatic polarization system. A glassy-carbon electrode and a platinum wire were used as working and counter electrodes, respectively, with an Ag/Ag^+ reference electrode used at −50 °C in all the experiments. The correction of the reference electrode was evaluated by standard procedures and referenced against the ferrocene/ferrocenium redox couple. Resonance Raman spectra were obtained with a polychromator (MC-100DG, Ritsu Oyo Kogaku), a Kr^+ laser (BeamLok 2060, Spectra-Physics) for 413.1 nm excitation, and a CCD detector (Symphony, CCD-1024x256-OPEN-1LS, HORIBA Jobin Yvon) cooled with liquid N_2. A holographic super notch filter (Kaiser Optical Systems) was used to minimize the Rayleigh scattering. Spectra of solvated samples were collected in spinning cells (0.5 cm diameter, 330 rpm) at −60 °C. The laser power was 20 mW. A 135° backscattering geometry was adopted, and the data accumulation time was 30 min. Peak frequencies were calibrated relative to indene standards (accurate to ±1 cm^{-1}).

2.3. Typical Experiment for Electrochemical Oxidation of Ni^{III}-Phenoxide Complexes. $[\mathbf{1}^{cn}]SbF_6$ (8.4 mg, 0.01 mmol) and tetra-*n*-butylammonium perchlorate (428 mg, 1.25 mmol) were dissolved in 50 mL of CH_2Cl_2 (0.2 mM). A 40 μL portion of pyridine (0.50 mmol) was added to the solution, and the resulting solution was oxidized by 1.2 V electrolysis at −78 °C. The oxidation process was checked by coulometry. When more than 0.95 electron was transferred from the complexes, the electrolysis was stopped and the resulting solution was identified by UV−vis−NIR absorption and resonance Raman spectroscopy as one-electron-oxidized Ni^{III}-phenoxide complexes.

2.4. Typical Experiment for Chemical Oxidation of Ni^{III}-Phenoxide Complexes with $[Ru(bpy)_3](PF_6)_3$. $[\mathbf{1}^{cn}]^+$ (3.4 mg, 0.004 mmol) was dissolved in 10 mL of CH_2Cl_2 (0.4 mM). To this solution was added 16 μL of pyridine (0.20 mmol), and the solution was cooled to −50 °C. The 4 mM CH_3CN solution of $[Ru(bpy)_3](PF_6)_3$ (1 mL, 0.004 mmol) was added to the solution at −50 °C.

2.5. XAS Experiments. The Ni K-edge XAS spectra were collected at the Stanford Synchrotron Radiation Laboratory under the ring condition of 3.0 GeV and ∼500 mA in top-off mode. The measurement utilized the 20-pole wiggler beamline 7-3 with unfocused beam and a Si(220) monochromator with ϕ = 90° alignment. The higher harmonic components from the monochromator were eliminated by a vertically collimating premonochromator harmonic rejection mirror. Solution samples were prepared in pinhole Delrin sample cells with 1 mil Kapton tape. The loaded cells were frozen by liquid nitrogen after a few seconds of mixing upon oxidation. The temperature of solution samples was maintained at 10 K during measurements using a dedicated Oxford liquid He flow cryostat. Incident (I0) and transmission (I1 and I2) beam intensities were measured using N_2-filled ion chambers at 1100 V potential. The data were collected in fluorescence mode using a 30-element Ge solid state detector (Canberra) with a Soller slit frame equipped with a 3 μm Co Z-1 filter. The Ni calibration foil was placed between the second (I1) and third (I2) ion chambers. The energy was calibrated by setting the first inflection point along the rising edge of the Ni-foil spectra to 8333.0 eV.[30] At least three spectra were averaged for XANES and EXAFS analyses. Only a negligible effect of radiation damage was observed during data normalization. The energy calibration and averaging of spectra were performed using SIXPACK.[31] The reduced data were processed for background subtraction, data renormalization, extraction of EXAFS oscillation, and collection of Fourier transform data using Athena.[32] For EXAFS analysis, the theoretical EXAFS scattering pathways were calculated by FEFF version 6.0[33] and used in Artemis.[32] The structural parameters were refined by allowing the pathway length (R) and the Debye−Waller factor to vary for each scattering path. Given the small difference in atomic number, we could not differentiate between Ni−O and Ni−N scattering pathways. The degeneracy of Ni−O/N scattering for $[\mathbf{1}^{cn}]^+$ and $[\mathbf{2}^{pn}]^+$ was set to 4, due to 4 comparable distances for Ni−O and Ni−N with salen-type ligands. The variations of the Ni−O and Ni−N bond lengths in complexes $[\mathbf{1}^{cn}]^+$ and $[\mathbf{2}^{pn}]^+$ are within 0.03 Å (Table 4). The EXAFS features of complexes $[\mathbf{1}^{cn}\text{-}\mathbf{py}]^+$ and $[\mathbf{2}^{pn}\text{-}\mathbf{py}]^+$ were fitted with an additional Ni−N distance with double degeneracy due to the presence

dx.doi.org/10.1021/ic501181k | Inorg. Chem. 2014, 53, 10195−10202

of the axially coordinated N of pyridine. The EXAFS of $[\mathbf{2}^{pn}\text{-}py]^{2+}$ were analyzed with fitting parameters similar to those used for $[\mathbf{1}^{cn}\text{-}py]^{2+}$ without being able to obtain a reasonable fit. The degeneracy of Ni−N/O−C multiple scattering pathways were also increased to accompany the C atom bonding to N of pyridine (Table 3). The numbers of independent points for EXAFS analyses were calculated following $N_{ind} = (2(\Delta k)(\Delta R))/\pi$, where $\Delta R = 2$ and Δk was more than 7.65, and thus N_{ind} was more than 9.7. The number of variables was maintained to be less than N_{ind}.

2.6. Calculation Details. Geometry optimizations were performed using the Gaussian 09 program (Revision D.01),[34] the B3LYP functional,[35,36] the 6-31g(d) basis set, and a polarized continuum model (PCM) for CH_2Cl_2 (dielectric $\varepsilon = 8.94$).[37] This functional/basis set combination has been shown previously to give the best agreement with solid-state structural data for this class of compounds.[10,16,38] Frequency calculations at the same level of theory confirmed that the optimized structures were located at a minimum on the potential energy surface. Single-point calculations for energetic analysis were performed using the BLYP[39] functional, the 6-311g(d) basis set, and a polarized continuum model (PCM) for CH_2Cl_2 (dielectric $\varepsilon = 8.94$).[36] For the one-electron-oxidized Ni(III) complexes the fragment guess function in Gaussian was used to search for plausible electronic structures for the complexes. The resulting electronic solutions are detailed in the Supporting Information (Tables S2−S4), and in many cases different initial guesses converged to a common electronic structure.

3. RESULTS AND DISCUSSION

3.1. Preparation and Characterization of Precursor Ni^{III}-Phenoxide Complexes. Previously we and others reported that addition of exogenous ligands, such as pyridine, to a solution of Ni^{II}-phenoxyl radical complexes of salen-type ligands affords Ni^{III}-phenoxide complexes with a six-coordinate geometry, and the association constants (log β) were estimated to be 7.3 ± 0.2, 6.8 ± 0.2, and 7.3 ± 0.2 M^{-2} at 223 K for $[\mathbf{1}^{cn}]^+$, $[\mathbf{1}^{en}]^+$, and $[\mathbf{2}^{pn}]^+$, respectively (Figure S1, Supporting Information). Further addition of pyridine (up to 50 equiv) to solutions of the Ni^{II}-phenoxyl radical complexes did not result in further spectral changes; therefore, the Ni^{III}-phenoxide complexes were prepared by addition of 50 equiv of pyridine to the Ni^{II}-phenoxyl radical species in CH_2Cl_2 below 223 K.[16,17] Cyclic voltammograms of all Ni^{III} complexes in CH_2Cl_2 exhibited one reversible redox wave (0.85 V for $[\mathbf{1}^{cn}\text{-}py]^+$, 0.82 V for $[\mathbf{1}^{en}\text{-}py]^+$, and 0.46 V for $[\mathbf{2}^{pn}\text{-}py]^+$ versus Fc/Fc^+) in the higher range from the rest potential (0.39, 0.46, and 0.37 V for $[\mathbf{1}^{cn}\text{-}py]^+$ $[\mathbf{1}^{en}\text{-}py]^+$, and $[\mathbf{2}^{pn}\text{-}py]^+$, respectively) (Figure 1, Table 1). The CVs of the Ni^{III} complexes were different from those of the precursor Ni^{II} complexes **1** and **2**[15,17] due to differences in the oxidation state, coordination number, and geometry. The redox potential of $[\mathbf{2}^{pn}\text{-}py]^+$ is similar to the first ligand-based redox potential of complexes **1** and **2**, suggesting that $[\mathbf{2}^{pn}\text{-}py]^+$ may show a similar ligand-centered oxidation process in comparison to complexes **1** and **2**. On the other hand, the oxidation potential of the five-membered chelate complexes $[\mathbf{1}\text{-}py]^+$ (both cn and en) are ca. 0.3 V higher than that of $[\mathbf{2}^{pn}\text{-}py]^+$, suggesting that the oxidation locus of $[\mathbf{1}\text{-}py]^+$ may be different from that of $[\mathbf{2}^{pn}\text{-}py]^+$.

3.2. Formation and Properties of One-Electron-Oxidized Ni^{III} Species. Electrochemical oxidation of the five-membered chelate complexes $[\mathbf{1}^{cn}\text{-}py]^+$ and $[\mathbf{1}^{en}\text{-}py]^+$ at 1.2 V and $[\mathbf{2}^{pn}\text{-}py]^+$ at 1.0 V in CH_2Cl_2 solution at −80 °C revealed a transfer of more than 0.9 electron per molecule with a gradual color change to dark red and purple for $[\mathbf{1}\text{-}py]^{2+}$ and $[\mathbf{2}\text{-}py]^{2+}$, respectively. The UV−vis−NIR spectra of the one-electron-oxidized species exhibited characteristic new peaks

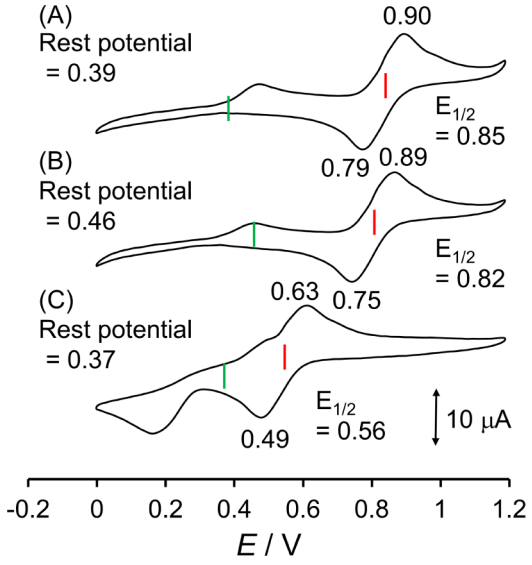

Figure 1. Cyclic voltammograms for Ni^{III} complexes (A) $[\mathbf{1}^{cn}\text{-}py]^+$, (B) $[\mathbf{1}^{en}\text{-}py]^+$, and (C) $[\mathbf{2}^{pn}\text{-}py]^+$. Conditions: in CH_2Cl_2, 223 K, 0.1 M $[NBu_4]ClO_4$ as the supporting electrolyte, a carbon electrode as the working electrode, a Pt electrode as the counter electrode, a Ag/Ag^+ electrode as the reference electrode, scan rate 100 mV/s.

Table 1. CV Data for Ni-salen Type Complexes

complex	$[\mathbf{1}^{cn}]$	$[\mathbf{1}^{cn}\text{-}py]^{+a}$	$[\mathbf{1}^{en}]$	$[\mathbf{1}^{en}\text{-}py]^{+a}$	$[\mathbf{2}^{pn}]$	$[\mathbf{2}^{pn}\text{-}py]^{+a}$
$E_{1/2}$ (V)	0.69	0.85	1.05	0.82	0.85	0.56
ref	14		40		16	

[a]Conditions: 1 mM complex, 0.1 M NBu_4ClO_4, scan rate 100 mV s^{-1}, CH_2Cl_2, 223 K.

(Figure 2, Table 2). Chemical oxidation by $[Ru^{III}(bpy)_3](PF_6)_3$[41] afforded the same oxidized species as for electro-

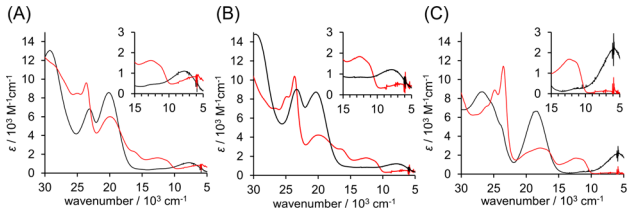

Figure 2. UV−vis−NIR spectral changes from Ni^{III}-phenoxide complexes to one-electron-oxidized forms using controlled electrolysis: (A) $[\mathbf{1}^{cn}\text{-}py]^+$ (black line), $[\mathbf{1}^{cn}\text{-}py]^{2+}$ (red line); (B) $[\mathbf{1}^{en}\text{-}py]^+$ (black line), $[\mathbf{1}^{en}\text{-}py]^{2+}$ (red line); (C) $[\mathbf{2}^{pn}\text{-}py]^+$ (black line), $[\mathbf{2}^{pn}\text{-}py]^{2+}$ (red line). Conditions: 223 K, 0.1 mM solution, 1 cm cell.

chemical oxidation (Figure S2, Supporting Information), as concluded from the similarity of the absorption spectra in the visible and NIR regions. In the UV−vis region, we only observed small differences in the spectra; those of the 5-chelate dinitrogen complexes $[\mathbf{1}^{cn}\text{-}py]^{2+}$ and $[\mathbf{1}^{en}\text{-}py]^{2+}$ were essentially the same. On the other hand, a notable difference is observed in the NIR region, where a weak band was observed at ca. 6000 cm^{-1} (ε = 500−800 $M^{-1}cm^{-1}$) for the five-membered chelate complexes $[\mathbf{1}\text{-}py]^{2+}$ but $[\mathbf{2}^{pn}\text{-}py]^{2+}$ showed no significant NIR bands. The variation in the NIR spectral features suggests a difference in the detailed electronic structures of the oxidized complexes, such as a difference in oxidation locus, metal versus ligand, and localization and delocalization of the oxidation

dx.doi.org/10.1021/ic501181k | Inorg. Chem. 2014, 53, 10195−10202

Table 2. UV−Vis−NIR Data of $[1^{cn}\text{-py}]^{n+}$, $[1^{en}\text{-py}]^{n+}$, and $[2^{pn}\text{-py}]^{n+}$ (n = 1, 2)

complex	ν/cm^{-1} (ε/M^{-1} cm^{-1})
$[1^{cn}\text{py}]^{+}$	29300 (12800), 22900 (6900), 19900 (8700), 12600 (400), 7600 (1100)
$[1^{cn}\text{-py}]^{2+}$	28200 (9100), 25000 (8000), 23500 (10100), 19100 (5100), 15900 (2600), 12200 (1800), 5900 (800)
$[1^{en}\text{-py}]^{+}$	23100 (9000), 20200 (8700), 7700 (1200)
$[1^{en}\text{-py}]^{2+}$	26800 (6800), 24800 (8200), 23500 (10100), 19500 (4200), 16000 (2500), 12200 (1800), 6000 (500)
$[2^{pn}\text{-py}]^{+}$	26900 (8500), 25600 (7300), 23800 (5200), 18500 (6700), 11400 (200), 6000 (2200)
$[2^{pn}\text{-py}]^{2+}$	26700 (7100), 24800 (8900), 23400 (11200), 17600 (2800), 11200 (1400)

locus. The UV−vis−NIR and CV results suggest that the electronic structures of the one-electron-oxidized Ni^{III} complexes differ depending on the chelate ring size.

The oxidized species could be reduced to the original Ni^{III}-phenoxide species by addition of 1 equiv of ferrocene. This result indicated the reversibility of the redox process, which is in good agreement with the observation of a reversible redox wave by CV (Figure S3, Supporting Information).

All three oxidized Ni^{III} complexes were X-band EPR silent at 4 K in the range 0−500 mT (Figure S4, Supporting Information), suggesting an electronic structure different from that of the Ni^{III} species, which has characteristic EPR signals of axially symmetrical S = 1/2 at g_{av} = ca. 2.15.[42] These EPR data suggest either that there is antiferromagnetic coupling of the radical spins in oxidized Ni^{III}-radical species or that the triplet energy difference is outside of the range of X-band EPR. An S = 0 ground state has been measured for a large number of Ni bis-ligand radical systems, with the strength of antiferromagnetic coupling dependent on the degree of exchange through the central metal ion.[6,28,43]

3.3. XAS Analyses. In order to experimentally evaluate the changes in the nickel oxidation states and the nickel coordination geometry of five- and six-membered chelate ring complexes, we carried out nickel K-edge X-ray absorption spectroscopic (XAS) measurements for frozen solutions at 10 K. The Ni pre-edge (1s to 3d transition) and rising edge (1s to 4p transition) for the Ni^{II} phenoxyl radical complexes $[1^{cn}]^{+}$ and $[2^{pn}]^{+}$ and their corresponding Ni^{III} pyridine adducts $[1^{cn}\text{-py}]^{+}$ and $[2^{pn}\text{-py}]^{+}$ (Figure 3, Table 3) showed distinct differences, which are attributable to a change in the metal oxidation state from Ni^{II} to Ni^{III} upon oxidation.[44] The disappearance of a well-defined shoulder along the rising edge further suggests the increase in the coordination number from 4 to 6.[44,45] The change in the pre-edge feature position (from 8333.8 eV for $[1^{cn}]^{+}$ to 8335.1 eV for $[1^{cn}\text{-py}]^{+}$ and from 8333.4 eV for $[2^{pn}]^{+}$ to 8334.2 eV for $[2^{pn}\text{-py}]^{+}$) (Table 3) is due to the combined effect of increasing the Ni effective nuclear charge by a metal-centered oxidation and the change from square-planar to octahedral coordination.[44] The rising-edge inflection points as a measurement of Ni effective nuclear charge at 8346.5 and 8346.6 eV for $[1^{cn}\text{-py}]^{+}$ and $[1^{cn}\text{-py}]^{2+}$, respectively, are practically identical. Similarly, the pre-edge features for $[1^{cn}\text{-py}]^{+}$ and $[1^{cn}\text{-py}]^{2+}$ (8334.9 eV) showed no significant shift. These results indicate that the oxidation locus is not metal-based for this derivative. On the other hand, $[2^{pn}\text{-py}]^{2+}$ exhibited counterintuitive changes in rising-edge and pre-edge energy positions relative to $[2^{pn}\text{-py}]^{+}$, with a shift to lower energy by 0.7 and 0.8 eV, respectively (pre-edge, 8333.4 eV in $[2^{pn}\text{-py}]^{2+}$ versus 8334.2 eV $[2^{pn}\text{-py}]^{+}$; rising edge, 8345.4 eV in $[2^{pn}\text{-py}]^{2+}$ versus 8346.1 eV $[2^{pn}\text{-py}]^{+}$) (Table 3). These spectral changes suggest a decrease in the Ni effective nuclear charge upon oxidation. The ca. 0.7 eV differences are in good agreement with the XAS differences between six-coordinated $[Ni^{II}(cyclam)Cl_2]$ and $[Ni^{III}(cyclam)Cl_2]^{+}$.[44] Therefore, the oxidation locus on $[2^{pn}\text{-py}]^{2+}$ is the ligand, which concomitantly reduces the Ni^{III} center to form a Ni^{II}-bis(phenoxyl radical) complex.

Extended X-ray absorption fine structure (EXAFS) analyses revealed different coordination geometries for $[1^{cn}\text{-py}]^{2+}$ and $[2^{pn}\text{-py}]^{2+}$. For the Ni^{III} complexes $[1^{cn}\text{-py}]^{+}$ and $[2^{pn}\text{-py}]^{+}$ the four N/O donors of the salen ligand and the two N donors of the pyridines could be fit with two single-scattering shells at distances of 1.88 and 2.20 Å for $[1^{cn}\text{-py}]^{+}$ and 1.91 and 2.12 Å for $[2^{pn}\text{-py}]^{+}$, respectively (Figure 4, Table 4). The EXAFS structure of $[1\text{-py}]^{2+}$ with four N/O donors at 1.93 Å and two

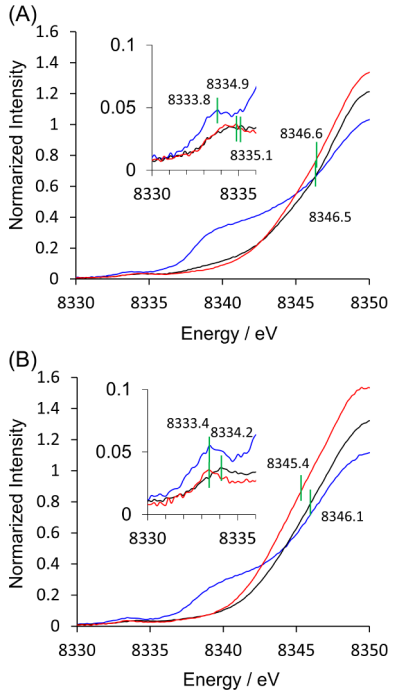

Figure 3. XANES of four-coordinate Ni^{II}-phenoxyl radical and six-coordinate Ni^{III}-phenolate and their oxidized complexes and expansion of the pre-edge region (inset): (A) $[1^{cn}]^{+}$ (blue line), $[1^{cn}\text{-py}]^{+}$ (black line), $[1^{cn}\text{-py}]^{2+}$ (red line); (B) $[2^{pn}]^{+}$ (blue line), $[2^{pn}\text{-py}]^{+}$ (black line), $[2^{pn}\text{-py}]^{2+}$ (red line).

Table 3. XANES and EXAFS Data of Ni Complexes

	pre-edge energy (eV) (intensity)	rising-edge energy (eV)	ligation	R (Å)	σ (Å^2)
$[1^{cn}]$	8334.1 (0.054)	8338.9	4 N/O	1.84	0.00263
$[1^{cn}]^{+}$	8333.8 (0.048)	8339.1	4 N/O	1.83	0.00216
$[1^{cn}\text{-py}]^{+}$	8335.1 (0.036)	8346.5	4 N/O	1.88	0.00366
			2 N	2.20	0.00176
$[1^{cn}\text{-py}]^{2+}$	8334.9 (0.037)	8346.6	4 N/O	1.93	0.00617
			2 N	2.16	0.00112
$[2^{pn}]$	8333.7 (0.053)	8338.8	4 N/O	1.87	0.00647
$[2^{pn}]^{+}$	8333.4 (0.055)	8339.2	4 N/O	1.86	0.00730
$[2^{pn}\text{-py}]^{+}$	8334.2 (0.037)	8346.1	4 N/O	1.91	0.00590
			2 N	2.12	0.00158
$[2^{pn}\text{-py}]^{2+}$	8333.4 (0.036)	8345.4	6 N/O	2.06	0.00413

dx.doi.org/10.1021/ic501181k | Inorg. Chem. 2014, 53, 10195−10202

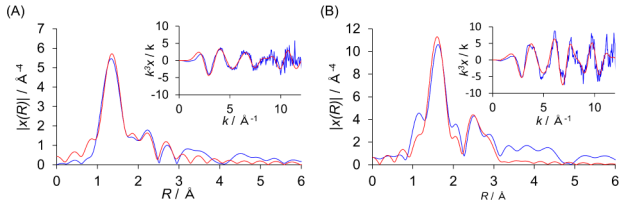

Figure 4. EXAFS data (blue line) and fits (red line) of R space and k space (inset): (A) $[\mathbf{1}^{cn}\text{-}py]^{2+}$; (B) $^{pn}\text{-}py]^{2+}$.

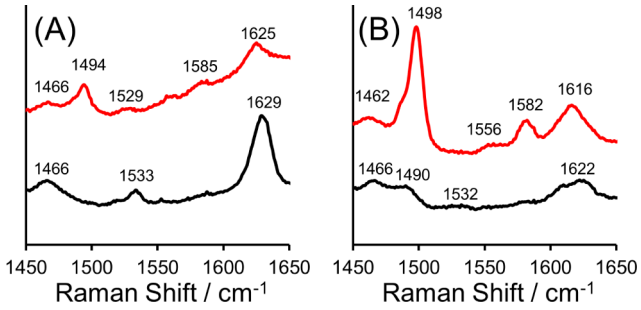

Figure 5. Resonance Raman spectral changes from Ni^{III} complexes to one-electron-oxidized species (λ_{ex} 413.1 nm, CH_2Cl_2 at −60 °C): (A) $[\mathbf{1}^{en}\text{-}py]^{+}$ (black line), $[\mathbf{1}^{en}\text{-}py]^{2+}$ (red line); (B) $[\mathbf{2}^{pn}\text{-}py]^{+}$ (black line), $[\mathbf{2}^{pn}\text{-}py]^{2+}$ (red line).

N donors at 2.16 Å was very similar to that of $[\mathbf{1}\text{-}py]^{+}$. The slight elongation of the distances for the 4-donors in the equatorial plane parallels the observed elongation of the metal−phenoxyl radical bond relative to the metal−phenolate bond and an overall expansion of the salen coordination sphere, as shown for the localized phenoxyl radical species.[46,47] On the other hand, $[\mathbf{2}^{pn}\text{-}py]^{2+}$ showed a local coordination geometry different from that of $[\mathbf{2}^{pn}\text{-}py]^{+}$, with all six Ni−N/O distances being best modeled at 2.06 Å.[48] This structural feature closely matches the general M−L bond lengths of high-spin octahedral Ni^{II} rather than Ni^{III} species.[49] From these results, we assigned $[\mathbf{1}^{cn}\text{-}py]^{2+}$ as a Ni^{III}-monophenoxyl radical complex and $[\mathbf{2}^{pn}\text{-}py]^{2+}$ as a high-spin Ni^{II}-bis(phenoxyl radical) complex.

3.4. Resonance Raman Analysis. Resonance Raman spectra of the oxidized complexes $[\mathbf{1}^{en}\text{-}py]^{2+}$, $[\mathbf{1}^{cn}\text{-}py]^{2+}$, and $[\mathbf{2}^{pn}\text{-}py]^{2+}$ exhibited the characteristic phenoxyl radical ν_{7a} band[13,28,50] at 1494, 1493, and 1498 cm^{-1}, respectively (Figure 5 and Figure S6 (Supporting Information)), suggesting that the oxidized complexes $[\mathbf{1}\text{-}py]^{2+}$ and $[\mathbf{2}^{pn}\text{-}py]^{2+}$ could be assigned to phenoxyl radical species. Although the intensities of the ν_{7a} bands for $[\mathbf{1}^{en}\text{-}py]^{2+}$ and $[\mathbf{1}^{cn}\text{-}py]^{2+}$ were very similar, the intensity of the phenoxyl radical ν_{7a} band of $[\mathbf{2}^{pn}\text{-}py]^{2+}$ was more intense in comparison to that of $[\mathbf{1}\text{-}py]^{2+}$. The intensity difference of the ν_{7a} band could arise from several factors. The UV−vis absorption spectra of all the oxidized Ni^{III} complexes around the excitation wavelength (λ_{ex} 413.1 nm) exhibited very similar absorption features, but the ε value of $[\mathbf{2}^{pn}\text{-}py]^{2+}$ is slightly larger (Table 2). The Raman band intensity of $[\mathbf{2}^{pn}\text{-}py]^{2+}$ may be enhanced due to the more intense absorption band around the excitation wavelength. On the other hand, the number of phenoxyl radicals in $[\mathbf{1}\text{-}py]^{2+}$ and $[\mathbf{2}^{pn}\text{-}py]^{2+}$ could be also considered; the five-membered chelate complexes $[\mathbf{1}\text{-}py]^{2+}$ contain one phenoxyl radical moiety, while the six-membered chelate complex $[\mathbf{2}^{pn}\text{-}py]^{2+}$ can be described as a bis(phenoxyl radical).[29] In addition, the phenolate ν_{11a} band at 1529 and 1527 cm^{-1} remained in both $[\mathbf{1}^{en}\text{-}py]^{2+}$ and $[\mathbf{1}^{cn}\text{-}py]^{2+}$, but the band could not be detected in $[\mathbf{2}^{pn}\text{-}py]^{2+}$. The bands observed for $[\mathbf{1}\text{-}py]^{2+}$ suggested that $[\mathbf{1}\text{-}py]^{2+}$ can be assigned to a localized phenoxyl radical species, described as Ni^{III}-(phenolate)(phenoxyl radical). A similar observation was also reported for a one-electron-oxidized Cu^{II} salen-type complex, which exhibits a localized phenoxyl radical.[12] On the other hand, disappearance of the phenoxide band in $[\mathbf{2}^{pn}\text{-}py]^{2+}$ suggests that two phenoxide moieties were oxidized to a bis(phenoxyl radical) species. The bis(phenoxyl radical) state in $[\mathbf{2}^{pn}\text{-}py]^{2+}$ led to the intense ν_{7a} phenoxyl radical Raman band of the complex in comparison to that of $[\mathbf{1}\text{-}py]^{2+}$. From these results, the complex $[\mathbf{2}^{pn}\text{-}py]^{2+}$ was assigned as Ni^{II}-bis(phenoxyl radical), which is in line with the assignment from the XAS analyses.

3.5. Theoretical Calculations. Density functional theory (DFT) calculations on the complexes $[\mathbf{1}^{cn}\text{-}py]^{+}$, $[\mathbf{1}^{en}\text{-}py]^{+}$, and $[\mathbf{2}^{pn}\text{-}py]^{+}$ and their oxidized analogues were undertaken to better understand the electronic structures. The predicted geometries and electronic structures for the complexes $[\mathbf{1}^{cn}\text{-}py]^{+}$ and $[\mathbf{1}^{en}\text{-}py]^{+}$, containing five-membered chelate backbones, and their oxidized forms were found to be essentially identical (Figures S7−S13 and Tables S1−S3, Supporting Information). We have thus focused the discussion on the cyclohexyl backbone analogue and comparison to the propyl backbone derivative, in order to compare the predicted metrical parameters with the EXAFS fitting. The predicted metrical parameters for $[\mathbf{1}^{cn}\text{-}py]^{2+}$ and $[\mathbf{2}^{pn}\text{-}py]^{2+}$ (starting from the optimized $[\mathbf{1}^{cn}\text{-}py]^{+}$ and $[\mathbf{2}^{pn}\text{-}py]^{+}$ geometries, respectively) reproduced well the coordination sphere bond lengths, including the structural changes upon oxidation to the dications $[\mathbf{1}^{cn}\text{-}py]^{2+}$ and $[\mathbf{2}^{pn}\text{-}py]^{2+}$ (Table 4 and Figures 6 and 7). At the B3LYP[36]/6-31g(d) level of theory for all atoms, the Ni coordination distances predicted by geometry optimization of $[\mathbf{1}^{cn}\text{-}py]^{+}$ and $[\mathbf{1}^{cn}\text{-}py]^{2+}$ and of $[\mathbf{2}^{pn}\text{-}py]^{+}$ and $[\mathbf{2}^{pn}\text{-}py]^{2+}$ matched those of the EXAFS analyses within 0.024 Å for distances of the 4N/O nickel donors. Energetic analysis at the

Table 4. Comparison of the EXAFS Fitting Data with DFT Calculations

	EXAFS		DFT		
	Ni−N/O (Å)	Ni−N_{py} (Å)	Ni−O (Å)	Ni−N_{sal} (Å)	Ni−N_{py} (Å)
$[\mathbf{1}^{cn}]^{+}$	1.83		1.844	1.841	
$[\mathbf{1}^{cn}\text{-}py]^{+}$	1.88	2.20	1.886/1.887	1.899/1.902	2.266/2.268
$[\mathbf{1}^{cn}\text{-}py]^{2+}$	1.93	2.16	1.963/1.856	1.910/1.907	2.171/2.301
$[\mathbf{1}^{en}\text{-}py]^{+}$			1.885/1.886	1.898/1.891	2.277/2.240
$[\mathbf{1}^{en}\text{-}py]^{2+}$			1.960/1.853	1.904/1.900	2.173/2.280
$[\mathbf{2}^{pn}]^{+}$	1.86		1.851	1.870	
$[\mathbf{2}^{pn}\text{-}py]^{+}$	1.91	2.12	1.897	1.935	2.270
$[\mathbf{2}^{pn}\text{-}py]^{2+}$	2.06	2.06	2.064	2.043	2.180

dx.doi.org/10.1021/ic501181k | Inorg. Chem. 2014, 53, 10195−10202

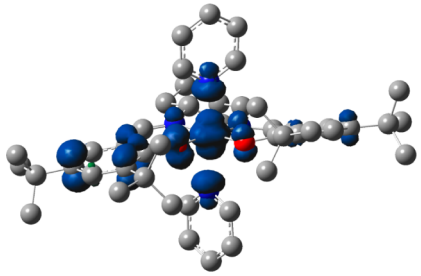

Figure 6. Predicted spin density plot for the $S = 1$ solution for $[\mathbf{1}^{cn}\text{-}\mathbf{py}]^{2+}$ corresponding to a Ni^{III}-phenoxyl radical structure. See the Experimental Section for calculation details.

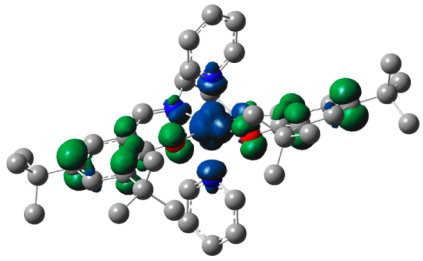

Figure 7. Predicted spin density plot for the ground state for $[\mathbf{2}^{pn}\text{-}\mathbf{py}]^{2+}$, showing an antiferromagnetically coupled Ni^{II}-bis(phenoxyl radical) species. See the Experimental Section for calculation details.

BLYP[39]/6-311g(d) level of theory revealed a number of electronic states for $[\mathbf{1}^{cn}\text{-}\mathbf{py}]^{2+}$ (Table S2, Supporting Information); however, the electronic ground state is predicted to be a low-spin d^7 Ni^{III} localized phenoxyl radical electronic solution ($S = 1$, Figure 6), which also provides the best geometric match to the EXAFS data. The assignment of $[\mathbf{1}^{cn}\text{-}\mathbf{py}]^{2+}$ as a Ni^{III} localized phenoxyl radical by a combination of spectroscopic methods and theoretical calculations agrees well with the lower intensity of the NIR band of $[\mathbf{1}^{cn}\text{-}\mathbf{py}]^{2+}$ at 5900 cm^{-1} and $[\mathbf{1}^{en}\text{-}\mathbf{py}]^{2+}$ at 6000 cm^{-1} (Figure 2), in comparison to the delocalized Ni^{II}-monophenoxyl radical $[\mathbf{1}^{cn}]^{+}$,[13,51] suggesting a phenolate to phenoxyl radical transition described as class II localization by the Robin and Day classification.[11,12,52,53]

The DFT calculations for $[\mathbf{2}^{pn}\text{-}\mathbf{py}]^{2+}$ resulted in a number of electronic solutions of similar energy; however no Ni^{III} ligand radical electronic solution was located for the propyl backbone (Table S4, Supporting Information). The calculated electronic ground state for the complex $[\mathbf{2}^{pn}\text{-}\mathbf{py}]^{2+}$ was an antiferromagnetically coupled Ni^{II}-bis(phenoxyl radical) species (Figure 7). An electronic solution consisting of a high-spin Ni^{II} center ferromagnetically coupled to two phenoxyl radicals (+1.4 kcal/mol) and a high-spin Ni^{II} center exhibiting one ferromagnetic and one antiferromagnetic interaction to two phenoxyl radicals (+0.6 kcal/mol) was slightly higher in energy (Table S4). The calculated high-spin Ni^{II}-bis(phenoxyl radical) electronic structure for $[\mathbf{2}^{pn}\text{-}\mathbf{py}]^{2+}$ is in good agreement with the interpretation of the resonance Raman, the pre-edge, and the EXAFS structural features of $[\mathbf{2}^{pn}\text{-}\mathbf{py}]^{2+}$. In addition, $[\mathbf{2}^{pn}\text{-}\mathbf{py}]^{2+}$ exhibited no significant bands in the NIR region, which was in accord with the assigned electronic structure.[28,50]

4. CONCLUSION

We have characterized the one-electron-oxidized Ni^{III} complexes of salen-type ligands containing five- and six-membered dinitrogen chelate rings. The difference in the ring size led to a different oxidation locus of the one-electron-oxidized Ni^{III} complexes due to the ligand flexibility. The complexes with a five-membered chelate ring $[\mathbf{1}\text{-}\mathbf{py}]^{2+}$ could be assigned to a Ni^{III}-phenoxyl radical species, while the six-membered chelate complex $[\mathbf{2}^{pn}\text{-}\mathbf{py}]^{2+}$ was concluded to be a high-spin d^8 Ni^{II}-bis(phenoxyl radical) species. The more rigid coordination environment of the five-membered chelate ligands salen and salcn in $[\mathbf{1}\text{-}\mathbf{py}]^{2+}$ likely provides coordinate bond lengths that stabilize the Ni^{III} oxidation state. On the other hand, the increased flexibility of the six-membered chelate in $[\mathbf{2}^{pn}\text{-}\mathbf{py}]^{2+}$ stabilizes the bis-phenoxyl radical species, and the longer coordination sphere bond lengths associated with this form, in comparison to $[\mathbf{1}\text{-}\mathbf{py}]^{2+}$. The difference of oxidation locus depending on the chelate ring size was also observed in one-electron-oxidized Cu^{II} salen-type complexes.[12] The observed metal-centered reduction in the course of the one-electron oxidation is rare.[54] As an extension of the studies on the oxidation chemistry of nickel and other transition-metal salen-type complexes, further investigations of the high-valent nickel complexes are in progress in our laboratories.

■ ASSOCIATED CONTENT

Ⓢ Supporting Information

UV−vis−NIR spectral change for formation of Ni(III) complexes by addition of pyridine (Figure S1), UV−vis−NIR spectra of oxidized Ni(III) complexes by Ru(III) oxidation (Figure S2), UV−vis−NIR spectral change for chemical reduction of oxidized Ni(III) species (Figure S3), EPR of oxidized Ni(III) complexes (Figure S4), EXAFS data of Ni(III) and their oxidized complexes (Figure S5), resonance Raman spectra of oxidized Ni(III) complexes (Figure S6), and DFT calculation data of Ni(III) and their oxidized complexes (Figures S7−S16, Tables S1−S5). This material is available free of charge via the Internet at http://pubs.acs.org.

■ AUTHOR INFORMATION

Corresponding Author

*E-mail for Y.S.: yshima@mx.ibaraki.ac.jp.

Present Address

[▽]Department of Analytical Chemistry, University of Pannonia, Veszprem, Hungary.

Notes

The authors declare no competing financial interest.

■ ACKNOWLEDGMENTS

This work was supported in part by Grants-in-Aid for Scientific Research (Nos. 22550055 and 25410060 to Y.S. and 25109540 to T.O.) from the Ministry of Education, Culture, Sports, Science, Cooperative Research in Joint Studies Programs at the Institute for Molecular Science, and Technology of Japan by the Cooperative Research Program of Network Joint Research Center for Materials and Devices (Institute for Materials Chemistry and Engineering, Kyushu University). T.S. thanks the NSERC for a Discovery Grant and Westgrid for access to computational resources. R.K.S. acknowledges his sabbatical leave from Montana State University and his current funding from the European Union and the State of Hungary, cofinanced by the European Social Fund in the framework of TÁMOP 4.2.4.A/2-11-1-2012-0001 "National Excellence Program". Use of the Stanford Synchrotron Radiation Lightsource, SLAC National Accelerator Laboratory, is supported by the U.S. Department of Energy, Office of Science, Office of Basic Energy Sciences under Contract No. DE-AC02-76SF00515.

REFERENCES

(1) Chirik, P. J.; Wieghardt, K. *Science* **2010**, 794−795.
(2) Thomas, F. In *Stable Radicals: Fundamentals and Applied Aspects of Odd Electron Compounds*; Hicks, R. G., Ed.; Wiley: Chichester, U.K., 2010; pp 281−316.
(3) Shimazaki, Y. *The Chemistry of Metal Phenolates*; Zabicky, J., Ed.; Wiley: Chichester, U.K., 2014; pp 593−667.
(4) Lyons, C. T.; Stack, T. D. P. *Coord. Chem. Rev.* **2013**, *257*, 528−540.
(5) (a) Stubbe, J.; van der Donk, W. A. *Chem. Rev.* **1998**, *98*, 705−762. (b) Whittaker, M. M.; Ballou, D. P.; Whittaker, J. W. *Biochemistry* **1998**, *37*, 8426−8436. (c) Jazdzewski, B. A.; Tolman, W. B. *Coord. Chem. Rev.* **2000**, *200−202*, 633−685. (d) Whittaker, J. W. *Chem. Rev.* **2003**, *103*, 2347−2363.
(6) (a) Chaudhuri, P.; Verani, C. N.; Bill, E.; Bothe, E.; Weyhermüller, T.; Wieghardt, K. *J. Am. Chem. Soc.* **2001**, *123*, 2213−2223. (b) Herebian, D.; Bothe, E.; Bill, E.; Weyhermüller, T.; Wieghardt, K. *J. Am. Chem. Soc.* **2001**, *123*, 10012−10023.
(7) Kaim, W. *Inorg. Chem.* **2011**, *50*, 9752−9765.
(8) (a) Shimazaki, Y.; Yamauchi, O. *Indian J. Chem.* **2011**, *50A*, 383−394. (b) Tezgerevska, T.; Alley, K. G.; Boskovic, C. *Coord. Chem. Rev.* **2014**, *268*, 23−40.
(9) Storr, T.; Verma, P.; Pratt, R. C.; Wasinger, E. C.; Shimazaki, Y.; Stack, T. D. P. *J. Am. Chem. Soc.* **2008**, *130*, 15448−15459.
(10) (a) Orio, M.; Jarjayes, O.; Kanso, H.; Philouze, C.; Neese, F.; Thomas, F. *Angew. Chem., Int. Ed.* **2010**, *49*, 4989−4992. (b) Kochem, A.; Jarjayes, O.; Baptiste, B.; Philouze, C.; Vezin, H.; Tsukidate, K.; Tani, F.; Orio, M.; Shimazaki, Y.; Thomas, F. *Chem. Eur. J.* **2012**, *18*, 1068−1072. (c) Kochem, A.; Kanso, H.; Baptiste, B.; Arora, H.; Philouze, C.; Jarjayes, O.; Vezin, H.; Luneau, D.; Orio, M.; Thomas, F. *Inorg. Chem.* **2012**, *51*, 10557−10571. (d) Cao, T-P-A.; Nocton, G.; Richard, L.; Goff, X. F. L.; Auffrant, A. *Angew. Chem., Int. Ed.* **2014**, *53*, 1368−1372.
(11) Kurahashi, T.; Fujii, H. *J. Am. Chem. Soc.* **2011**, *133*, 8307−8316.
(12) Asami, K.; Tsukidate, K.; Iwatsuki, S.; Tani, F.; Karasawa, S.; Chiang, L.; Storr, T.; Thomas, F.; Shimazaki, Y. *Inorg. Chem.* **2012**, *51*, 12450−12461.
(13) Shimazaki, Y.; Tani, F.; Fukui, K.; Naruta, Y.; Yamauchi, O. *J. Am. Chem. Soc.* **2003**, *125*, 10512−10513.
(14) Shimazaki, Y.; Yajima, T.; Tani, F.; Karasawa, S.; Fukui, K.; Naruta, Y.; Yamauchi, O. *J. Am. Chem. Soc.* **2007**, *129*, 2559−2568.
(15) Shimazaki, Y.; Stack, T. D. P.; Storr, T. *Inorg. Chem.* **2009**, *48*, 8383−8392.
(16) Storr, T.; Wasinger, E. C.; Pratt, R. C.; Stack, T. D. P. *Angew. Chem., Int. Ed.* **2007**, *46*, 5198−5201.
(17) Shimazaki, Y.; Arai, N.; Dunn, T. J.; Yajima, T.; Tani, F.; Ramogida, C. F.; Storr, T. *Dalton. Trans.* **2011**, *40*, 2469−2479.
(18) (a) Rotthaus, O.; Jarjayes, O.; Thomas, F.; Philouze, C.; Valle, C. P. D.; Saint-Aman, E.; Pierre, J.-L. *Chem. Eur. J.* **2006**, *12*, 2293−2302. (b) Rotthaus, O.; Jarjayes, O.; Philouze, C.; Valle, C. P. D.; Thomas, F. *Dalton. Trans.* **2009**, *38*, 1792−1800. (c) Ghorai, S.; Mukherjee, C. *Dalton Trans.* **2014**, *43*, 394−397.
(19) (a) Rotthaus, O.; Jarjayes, O.; Valle, C. P. D.; Philouze, C.; Thomas, F. *Chem. Commun.* **2007**, 4462−4464. (b) Kochem, A.; Orio, M.; Jarjayes, O.; Neese, F.; Thomas, F. *Chem. Commun.* **2010**, *46*, 6765−6767. (c) Chiang, L.; Kochem, A.; Jarjayes, O.; Dunn, T. J.; Vezin, H.; Sakaguchi, M.; Ogura, T.; Orio, M.; Shimazaki, Y.; Thomas, F.; Storr, T. *Chem. Eur. J.* **2012**, *18*, 14117−14127.
(20) Franks, M.; Gadzhiezva, A.; Ghandhi, L.; Murrell, D.; Blake, A. J.; Davies, E. S.; Lewis, W.; Moro, F.; McMaster, J.; Schröder, M. *Inorg. Chem.* **2013**, *52*, 660−670.
(21) Bag, B.; Mondal, N.; Rosair, G.; Mitra, S. *Chem. Commun.* **2000**, 1729−1730.
(22) (a) Martin, A. *Chem. Rev.* **2010**, *110*, 576−623. (b) Jana, R.; Pathak, T. P.; Sigman, M. S. *Chem. Rev.* **2011**, *111*, 1417−1492.
(23) Lippert, B. *In Cisplatin. Chemistry and Biochemistry of a Leading Anticancer Drug*; Lippert, B., Ed.; Verlag Helvetica Chimica Acta, Postfach: Zürich, 1999.
(24) Shimazaki, Y.; Yamauchi, O. *Chem. Biodivers.* **2012**, *9*, 1635−1658.
(25) Kostić, N. M.; Dutcă, L.-M. In *Comprehensive Coordination Chemistry II*; McCleverty, J. A., Meyer, T. J., Eds.; Elsevier: Sheffield, U.K., 2003; Vol. *6*, pp 555−672.
(26) (a) Martone, D. P.; Osvath, P.; Lappin, A. G. *Inorg. Chem.* **1987**, *26*, 3094−3100. (b) Fernandez, I.; Pedro, J. R.; Rosello, A. L.; Ruiz, R.; Ottenwaelder, X.; Journaux, Y. *Tetrahedron Lett.* **1998**, *39*, 2869−2872. (c) Patra, A. K.; Mukherjee, R. *Inorg. Chem.* **1999**, *38*, 1388−1393.
(27) (a) Ragsdale, S. W. *J. Inorg. Biochem.* **2007**, *101*, 1657−1666. (b) Ragsdale, S. W. *J. Biol. Chem.* **2009**, *284*, 18571−18575.
(28) (a) Bellefeuille, D.; Askari, M. S.; Lassalle-Kaiser, B.; Journaux, Y.; Aukauloo, A.; Orio, M.; Thomas, F.; Ottenwaelder, X. *Inorg. Chem.* **2012**, *51*, 12796−12804. (b) Kochem, A.; Chiang, L.; Baptiste, B.; Philouze, C.; Leconte, N.; Jarjayes, O.; Storr, T.; Thomas, F. *Chem. Eur. J.* **2012**, *18*, 14590−14593.
(29) Dunn, T. J.; Webb, M. I.; Hazin, K.; Verma, P.; Wasinger, E. C.; Shimazaki, Y.; Storr, T. *Dalton Trans.* **2013**, *42*, 3950−3956.
(30) Thompson, A. C.; Attwood, D. T.; Gullikson, E. M.; Howells, M. R.; Kortright, J. B.; Robinson, A. L.; Underwood, J. H.; Kim, K.-J.; Kirz, J.; Lindau, I.; Pianetta, P.; Winick, H.; Williams, G. P.; Scofield, J. H. In *X-ray Data Booklet, Center for X-ray Optics, Advanced Light Source*; E Thompson, A. C., Vaughan, D., Eds.; Lawrence Berekeley National Laboratory, University of California: Berkeley, CA, 2001.
(31) Webb, S. M. *Phys. Scr.* **2005**, *T115*, 1011−1014.
(32) Ravel, B.; Newville, M. *J. Synchrotron Radiat.* **2005**, *12*, 537−541.
(33) (a) Rehr, J. J.; Kas, J. J.; Vila, F. D.; Prange, M. P.; Jorissen, K. *Phys. Chem. Chem. Phys.* **2010**, *12*, 5503−5513. (b) Rehr, J. J.; Kas, J. J.; Prange, M. P.; Sorini, A. P.; Takimoto, Y.; Vila, F. D. *Comptes Rendus Physique.* **2000**, *10*, 548−559. (c) Rehr, J. J.; Albers, R. C. *Rev. Mod. Phys.* **2000**, *72*, 621−654.
(34) Frisch, M. J.; Trucks, G. W.; Schlegel, H. B.; Scuseria, G. E.; Robb, M. A.; Cheeseman, J. R.; Scalmani, G.; Barone, V.; Mennucci,; Petersson, G. A.; Nakatsuji, H.; Caricato, M.; Li, X.; Hratchian, H. P.; Izmaylov, A. F.; Bloino, J.; Zheng, G.; Sonnenberg, J. L.; Hada, M.; Ehara, M.; Toyota, K.; Fukuda, R.; Hasegawa, J.; Ishida, M.; Nakajima, T.; Honda, Y.; Kitao, O.; Nakai, H.; Vreven, T.; Montgomery, J. A., Jr.; Peralta, J. E.; Ogliaro, F.; Bearpark, M.; Heyd, J. J.; Brothers, E.; Kudin, K. N.; Staroverov, V. N.; Kobayashi, R.; Normand, J.; Raghavachari, K.; Rendell, A.; Burant, J. C.; Iyengar, S. S.; Tomasi, J.; Cossi, M.; Rega, N.; Millam, J. M.; Klene, M.; Knox, J. E.; Cross, J. B.; Bakken, V.; Adamo, C.; Jaramillo, J.; Gomperts, R.; Stratmann, R. E.; Yazyev, O.; Austin, A. J.; Cammi, R.; Pomelli, C.; Ochterski, J. W.; Martin, R. L.; Morokuma, K.; Zakrzewski, V. G.; Voth, G. A.; Salvador, P.; Dannenberg, J. J.; Dapprich, S.; Daniels, A. D.; Farkas, Ö.; Foresman, J. B.; Ortiz, J. V.; Cioslowski, J.; Fox, D. J. *Gaussian 09, Revision D.01*; Gaussian, Inc., Wallingford, CT, 2009.
(35) Becke, A. D. *J. Chem. Phys.* **1993**, *98*, 5648−5652.
(36) Stephens, P. J.; Devlin, F. J.; Chabalowski, C. F.; Frisch, M. J. *J. Phys. Chem.* **1994**, *98*, 11623−11627.
(37) (a) Barone, V.; Cossi, M.; Tomasi, J. *J. Chem. Phys.* **1997**, *107*, 3210−3221. (b) Barone, V.; Cossi, M.; Tomasi, J. *J. Comput. Chem.* **1998**, *19*, 404−417. (c) Miertus, S.; Scrocco, E.; Tomasi, J. *Chem. Phys.* **1981**, *55*, 117−129. (d) Tomasi, J.; Mennucci, B.; Cances, E. *J. Mol. Struct.* **1999**, *464*, 211−226.
(38) (a) Chiang, L.; Allan, L. E. N.; Alcantara, J.; Wang, M. C. P.; Storr, T.; Shaver, M. P. *Dalton Trans.* **2014**, *43*, 4295−4304. (b) Dunn, T. J.; Chiang, L.; Ramogida, C. F.; Hazin, K.; Webb, M. I.; Katz, M. J.; Storr, T. *Chem. Eur. J.* **2013**, *19*, 9606−9618.
(39) (a) Becke, A. D. *Phys. Rev. A* **1988**, *38*, 3098−3100. (b) Lee, C. T.; Yang, W. T.; Parr, R. G. *Phys. Rev. B* **1988**, *37*, 785−789.
(40) Rotthaus, O.; Thomas, F.; Jarjayes, O.; Philouze, C.; Saint-Aman, E.; Pierre, J.-L. *Chem. Eur. J.* **2006**, *12*, 6953−6962.
(41) Biner, M.; Bürgi, H.-B.; Ludi, A.; Röhr, C. *J. Am. Chem. Soc.* **1992**, *114*, 5197−5203.
(42) (a) Ottenwaelder, X.; Ruiz-Garcia, R.; Blondin, G.; Carasco, R.; Cano, J.; Lexa, D.; Journaux, Y.; Aukauloo, A. *Chem. Commun.* **2004**, 504−505. (b) Drago, R. S.; Baucom, E. I. *Inorg. Chem.* **1972**, *11*,

2064−2069. (c) Krüger, H. J.; Holm, R. H. *Inorg. Chem.* **1987**, *26*, 3645−3647.
(43) (a) Ray, K.; Weyhermüller, T.; Neese, F.; Wieghardt, K. *Inorg. Chem.* **2005**, *44*, 5345−5360. (b) Herebian, D.; Bothe, E.; Neese, F.; Weyhermüller, T.; Wieghardt, K. *J. Am. Chem. Soc.* **2003**, *125*, 9116−9128. (c) Herebian, D.; Wieghardt, K. E.; Neese, F. *J. Am. Chem. Soc.* **2003**, *125*, 10997−11005. (d) Lu, C. C.; Bill, E.; Weyhermüller, T.; Bothe, E.; Wieghardt, K. *J. Am. Chem. Soc.* **2008**, *130*, 3181−3197.
(44) Colpas, G. J.; Maroney, M. J.; Bagyinka, C.; Kumar, M.; Willis, W. S.; Suib, S. L.; Baidya, N.; Mascharak, P. K. *Inorg. Chem.* **1991**, *30*, 920−928.
(45) DuBois, J. L.; Mukherjee, P.; Stack, T. D. P.; Hedman, B.; Solomon, E. I.; Hodgson, K. O. *J. Am. Chem. Soc.* **2000**, *122*, 5775−5787.
(46) Storr, T.; Verma, P.; Shimazaki, Y.; Wasinger, E. C.; Stack, T. D. P. *Chem. Eur. J.* **2010**, *16*, 8980−8983.
(47) Shimazaki, Y. *Adv. Mater. Phys. Chem.* **2013**, *3*, 60−71.
(48) The EXAFS fitting of $[\mathbf{2}^{\mathbf{pn}}\text{-}\mathbf{py}]^{2+}$ with four Ni−N/O and two Ni−N scattering pathways could not be fit due to negative Debye−Waller factors.
(49) Mayer, F.; Kozlowski, H. In *Comprehensive Coordination Chemistry II*; McCleverty, J. A., Meyer, T. J., Eds.; Elsevier: Sheffield, U.K., 2003; Vol. *6*, pp 247−554.
(50) McGlashen, M. L.; Eads, D. D.; Spiro, T. G.; Whittaker, J. W. *J. Phys. Chem.* **1995**, *99*, 4918−4922.
(51) (a) D'Alessandro, D. M.; Keene, F. R. *Chem. Soc. Rev.* **2006**, *35*, 424−440. (b) Nelsen, S. F. *Chem. Eur. J.* **2000**, *6*, 581−588.
(52) Robin, M. B.; Day, P. *Adv. Inorg. Radiochem.* **1967**, *10*, 247−422.
(53) (a) Kurahashi, T.; Hiroshi, F. *Inorg. Chem.* **2013**, *52*, 3908−3919. (b) Kochem, A.; Thomas, F.; Jarjayes, O.; Gellon, G.; Philouze, C.; Weyhermüller, T.; Neese, F.; Gastel, M. *Inorg. Chem.* **2013**, *52*, 14428−14438.
(54) (a) Attia, A. S.; Pierpont, C. G. *Inorg. Chem.* **1995**, *34*, 1172−1179. (b) Miller, J. S.; Min, K. S. *Angew. Chem., Int. Ed.* **2009**, *48*, 262−272. (c) Pierpont, C. G. *Inorg. Chem.* **2011**, *50*, 9766−9772. (d) Rajput, A.; Sharma, A. K.; Barman, S. K.; Koley, D.; Steinert, M.; Mukherjee, R. *Inorg. Chem.* **2014**, *53*, 36−48.